

See discussions, stats, and author profiles for this publication at: <https://www.researchgate.net/publication/231391200>

# Sorption of CO, CH<sub>4</sub>, and N<sub>2</sub> in Alkali Metal Ion Exchanged Zeolite-X: Grand Canonical Monte Carlo Simulation and Volumetric Measurements

ARTICLE *in* INDUSTRIAL & ENGINEERING CHEMISTRY RESEARCH · MAY 2010

Impact Factor: 2.59 · DOI: 10.1021/ie901713m

---

CITATIONS

21

READS

62

## 3 AUTHORS:



[Renjith S. Pillai](#)

Université de Montpellier

32 PUBLICATIONS 187 CITATIONS

[SEE PROFILE](#)



[Govind Sethia](#)

Reliance Industries Limited

14 PUBLICATIONS 148 CITATIONS

[SEE PROFILE](#)



[Raksh Vir Jasra](#)

Reliance Industries Limited

327 PUBLICATIONS 5,508 CITATIONS

[SEE PROFILE](#)

# Sorption of CO, CH<sub>4</sub>, and N<sub>2</sub> in Alkali Metal Ion Exchanged Zeolite-X: Grand Canonical Monte Carlo Simulation and Volumetric Measurements

Renjith S. Pillai,<sup>†</sup> Govind Sethia, and Raksh V. Jasra\*,<sup>†</sup>

*Discipline of Inorganic Materials and Catalysis, Central Salt and Marine Chemical Research Institute (CSMCRI), Council of Scientific and Industrial Research (CSIR), Bhavnagar-364021, Gujarat, India,*

Sorption of CO, CH<sub>4</sub>, and N<sub>2</sub> in zeolite-X exchanged with different alkali metal ions was studied by volumetric measurements and Grand Canonical Monte Carlo simulation. CO and CH<sub>4</sub> sorption is observed to show higher sorption capacity than N<sub>2</sub> in all cation exchanged zeolite samples. The adsorption capacity of CO in alkali metal exchanged zeolites is observed to decrease on moving from LiX to CsX, whereas for the methane adsorption capacity varies in reverse order. The isosteric heat of sorption data show stronger interactions of CO and N<sub>2</sub> molecules with alkali metal ion exchanged zeolites. The isosteric heat of CH<sub>4</sub> show nearly same value (21–24 kJ/mol) for all alkali metal ion exchanged zeolites. Simulation of the CO and N<sub>2</sub> sorption in alkali metal zeolite -X clearly shows that the adsorbed CO and N<sub>2</sub> molecules are located in proximity to the extra-framework cations in the super cage. Simulated data of adsorption isotherms and heats of adsorption of CO, N<sub>2</sub>, and CH<sub>4</sub> in alkali metal ion exchanged zeolite-X agree reasonably well with the experimental results.

## 1. Introduction

CH<sub>4</sub> and CO separation from its mixture with N<sub>2</sub> is one of the industrially significant separation processes.<sup>1–6</sup> Some of the waste gases from the iron works, fertilizer plants and petrochemical industry contain CO and CH<sub>4</sub>. Such industrial waste gases can be used as raw material for fine chemical production if CO and CH<sub>4</sub> are recovered with requisite purity. The tail gas in ammonia plants consists of CO, CH<sub>4</sub>, and N<sub>2</sub>. CO is a main feedstock for the synthesis of CH<sub>3</sub>OH and CH<sub>3</sub>COOH. Similarly, CH<sub>4</sub> can be converted to synthesis gas via re-forming reactions.<sup>3,7</sup> The recovery of CH<sub>4</sub> from off gases is also relevant as this is one of the major contributors to the global warming with 20 times higher global warming potential than that of CO<sub>2</sub>.<sup>8</sup> Moreover, catalytic CH<sub>4</sub> combustion is becoming attractive route to produce cleaner energy, since it allows efficient and complete fuel burning at lower temperature than flame combustion.<sup>6,10,11</sup>

CO and CH<sub>4</sub> can be recovered by cryogenic separation, solution absorption and adsorptive separation. The liquefaction temperature of CO and N<sub>2</sub> are very close; therefore, cryogenic separation is energy intensive, making the process expensive.<sup>3,4</sup> The solution absorption process is applied in industries as a large scale recovery of CO but this process has limitations like availability of economically viable solvent, corrosion of container, intensive energy requirement to recover product gases. The adsorption separation is economical in medium scale separations. This process is not recommended for the large scale CO or CH<sub>4</sub> separations because of unavailability of suitable adsorbents. Thus, highly pure CO and CH<sub>4</sub> can become commercially viable on large scale by PSA provided promising adsorbent with high adsorption capacity and selectivity is available.<sup>3,12–14</sup>

The most commonly used zeolites for adsorptive separation are synthetic zeolite A, X, and Y.<sup>15–20</sup> Adsorptive properties of zeolites depend on their framework composition and nature of extra framework cations. The size of the cation plays a major

role in the adsorption capacity as well as adsorption selectivity of gases.<sup>15,16,21–26</sup> The molecular properties of adsorbate influence the adsorption capacity, selectivity, and heat of adsorption towards a particular adsorbent. The dipole moment, quadrupole moment, and polarizability of CO, N<sub>2</sub>, and CH<sub>4</sub> are quite different, so that the adsorption behavior of these molecules toward specific adsorbent is expected to be different.<sup>26</sup> Maurin et al.<sup>27</sup> and our recent publications<sup>19,23–25</sup> have reported experimental as well as theoretical measurement of N<sub>2</sub> adsorption in zeolite-X with various alkali and alkaline earth metal extra framework cations. Talu et al.<sup>28</sup> measured the CH<sub>4</sub> adsorption isotherm in alkali metal exchanged zeolite-X.

The present paper deals with understanding of adsorption of CO, CH<sub>4</sub>, and N<sub>2</sub> in the alkali metal ion exchanged zeolite-X using experimental adsorption measurements. Grand canonical Monte Carlo simulation study was carried out to have a deeper understanding about the nature of cation–molecule interactions and to develop suitable forcefield for simulation studies.

## 2. Experimental Section

**2.1. Materials.** Zeolite-X (with chemical composition Na<sub>88</sub>Al<sub>88</sub>Si<sub>104</sub>O<sub>384</sub>·220H<sub>2</sub>O) was supplied by Zeolites and Allied Products, Mumbai, India. The salts used for cation exchange include lithium chloride, potassium chloride, cesium chloride (s.d. fine Chemicals, India) and rubidium chloride (Sigma Aldrich). N<sub>2</sub> (99.999%), CH<sub>4</sub> (99.99%), CO (99.99%), and He (99.999%) from Inox Air Products, India, were used for the adsorption isotherm measurements.

**2.2. Cation Exchange.** The extra framework cations were introduced into the highly crystalline sodium form of the zeolite X, by the conventional method of cation exchange using aqueous salt solution. Typically, the zeolites were repeatedly treated with 0.5 M aqueous salt chloride solution of the exchanging cations with a solid/liquid ratio 1:80 at 353 K for 4 h. The residue was filtered, washed with hot distilled water, until the washings were free from chloride ions as tested by AgNO<sub>3</sub> solution and dried in air at room temperature for 24 h. The extent of the different cation exchange was determined by chemical analysis (ICP, Perkin-Elmer Instruments, Optima 2000DV) of sodium and exchanged cation of zeolites.

\* Corresponding author. E-mail: rvjasra@gmail.com; rakshvir.jasra@ril.com. Telephone: +91 265 6696313. Fax: +91 265 6693934.

<sup>†</sup> Present address: Reliance Technology Group, Vadodara Manufacturing Division, Reliance Industries Limited, Vadodara-391346, Gujarat, India.

**2.3. X-ray Powder Diffraction.** X-ray powder diffraction studies at ambient temperature of adsorbent samples were carried out using a Philips X'pert MPD system in the  $2\theta$  range of  $5$ – $65^\circ$  using Cu K $\alpha 1$  ( $\lambda = 1.54056 \text{ \AA}$ ). The diffraction patterns of the materials indicate that they are highly crystalline, showing reflections in the range of  $5$ – $35^\circ$  that is typical of zeolites. The percent crystallinity of the cation exchanged zeolites was determined from the X-ray diffraction pattern by considering the intensity of 10 major peaks. The sodium form of the zeolite was considered to be an arbitrary standard for the calculations.

**2.4. Activation and Isotherm Measurements.** The presence of water in the zeolite significantly affects the adsorption behavior of zeolites, therefore, the samples were initially dried at room temperature, followed by drying at 353 K for 24 h in an oven. Prior to adsorption measurements, the samples were activated *in situ* by heating to 673 K, at a rate of  $1 \text{ K min}^{-1}$  under vacuum ( $5 \times 10^{-3} \text{ mm Hg}$ ) for 8 h. The stability of zeolite structure has been checked after activation by X-ray diffraction. The diffraction patterns of the materials shows zeolite structure is not destroyed during activation as all the typical reflections in the range of  $2\theta = 5$ – $35^\circ$  are retained.

$\text{N}_2$ ,  $\text{CH}_4$ , and CO adsorption isotherms were measured at 288.2 and 303.2 K using a static volumetric system (Micromeritics ASAP 2020). Adsorption temperature was maintained ( $\pm 0.1 \text{ K}$ ) by circulating water from a constant temperature bath (Julabo F25, Germany). Requisite amount of the adsorbate gas was injected into the volumetric set up at volumes required to achieve a targeted set of pressures ranging from 0.1 to 850 mmHg. Three pressure transducers of capacities 1 mmHg (accuracy within 0.12% of the reading), 10 mmHg (accuracy within 0.15% of the reading), and 1000 mmHg (accuracy within 0.073% of full scale) were used for the pressure measurements. A minimum equilibrium interval of 5 s with a relative target tolerance of 5.0% of the targeted pressure and an absolute target tolerance of 5.000 mmHg were used to determine equilibrium for each measurement point. Minimum equilibrium intervals with 300 s were also carried out to determine equilibrium for each measurement point of CO,  $\text{CH}_4$ , and  $\text{N}_2$  adsorption in zeolite samples (see Supporting Information). The adsorption and desorption was completely reversible, and it is possible to remove the adsorbed gases by simple evacuation.

The pure component selectivity of gas A over gas B was calculated by using the equation

$$\alpha_{A/B} = [V_A/V_B]_{P,T} \quad (1)$$

where  $V_A$  and  $V_B$  are the volumes of gases A and B, respectively, adsorbed at any given pressure  $P$  and temperature  $T$ .

Isosteric heats of adsorption were calculated from the adsorption data collected at 288.2 and 303.2 K using the Clausius–Clapeyron equation,

$$-\Delta_{ad}H^\theta = R[\partial(\ln P)/\partial(1/T)]_0 \quad (2)$$

where  $R$  is the universal gas constant and  $\theta$  is the fraction of the adsorbed sites at a pressure  $P$  and temperature  $T$ . The errors in adsorption selectivity and heat of adsorption estimated from propagation of error method were 0.4%, and 0.5% respectively.

### 3. Computational Methodology

The Materials Studio Sorption program (Accelrys Software Inc.), utilizing grand canonical ensemble (fixed chemical potential) Monte Carlo simulation methods, was used for

computation of adsorption data. The simulations were performed in IBM MPro workstation running on the Windows platform.

The crystal structure of the X-faujasite systems with the alkali metal cations was modeled as follows.<sup>21,22,25–27</sup> The chemical composition  $\text{Si}_{104}\text{Al}_{88}\text{M}_{88}\text{O}_{384}$  ( $M^+ = \text{Li}^+, \text{Na}^+, \text{K}^+, \text{Rb}^+, \text{Cs}^+$ ) was considered in order to reproduce the Si/Al ratio of 1.18 of the investigated samples. The framework was built with a strictly ordered alternation of aluminum and silicon atoms in accordance with the Lowenstein's Al–O–Al avoidance rule. For NaX zeolite, the distribution defined by Zhu et al.<sup>22</sup> was selected corresponding to 30  $\text{Na}^+$  in sites I' located in the sodalite cage in front of the 6-ring window connected to the hexagonal prism, 28  $\text{Na}^+$  in sites II, and 30  $\text{Na}^+$  in sites III, 6-ring and 4-ring windows of the supercages, respectively. The distributions of the extra-framework cations for  $\text{LiX}^{29}$  and  $\text{KX}^{30}$  provided by recent reinvestigation of these crystal structures include the occupation of sites I', II, III, and III' for  $\text{Li}^+$  and sites I, I', II, III, and III' for  $\text{K}^+$ . The  $\text{Rb}^+$  and  $\text{Cs}^+$  exchanged structures were constructed by using the crystallographic data obtained from Lee et al.<sup>31</sup> and Ryu et al.<sup>32</sup> respectively.

The force field used for the gas adsorption simulations was modified version of the Cerius<sup>2</sup> Watanabe–Austin potential energy model.<sup>32–38</sup> The total energy of the zeolite framework and adsorbed molecules ( $U$ ) is expressed as the sum of the interactions energy between the adsorbate and zeolite ( $U_{AZ}$ ) and that between the adsorbates ( $U_{AA}$ ) molecules.

$$U = U_{AZ} + U_{AA} \quad (3)$$

Both  $U_{AZ}$  and  $U_{AA}$  are written as the sums of pair wise additive potentials,  $u_{ij}$  in the form

$$u_{ij} = 4\epsilon_{ij} \left[ \left( \frac{\sigma_{ij}}{r_{ij}} \right)^{12} - \left( \frac{\sigma_{ij}}{r_{ij}} \right)^6 \right] + \left( \frac{q_i q_j}{r_{ij}} \right) \quad (4)$$

where the first term is the repulsion-dispersion LJ potential, with  $\epsilon_{ij}$  and  $\sigma_{ij}$  corresponding to the parameter sets for each interacting pair that is obtained from  $\epsilon_i$  and  $\sigma_i$  of each species by using the Lorentz–Berthelot mixing rule<sup>28</sup> (i.e., a geometric combining rule for the energy and an arithmetic one for the atomic size:  $\epsilon_{ij} = (\epsilon_i \epsilon_j)^{1/2}$  and  $\sigma_{ij} = (\sigma_i + \sigma_j)/2$ ). The second term is the Coulombic contribution between point charges  $q_i$  and  $q_j$  separated by distance  $r_{ij}$ .

$\text{N}_2$  molecules are represented by a three site model, the two outer sites are separated by a distance  $l$  as point charges of equal magnitude  $q$  and the third site is located at the middle of the outer sites with a point charge  $-2q$ , ensuring molecular charge neutrality. For  $\text{N}_2$  model  $q = -0.40484e$ ,  $l = 1.098 \text{ \AA}$ ,  $\sigma_{\text{N}} = 3.318 \text{ \AA}$ , and  $\epsilon_{\text{N}} = 0.0724 \text{ kcal mol}^{-1}$  were taken.<sup>34,39</sup> For CO, we used an atomic point charge model in which the charges (in electron units) assigned to the carbon C (+0.107) and the oxygen O (−0.107) atoms. The CO molecule and charges were obtained by DFT calculation employ DMol3 with PW91 functional.<sup>40</sup> These charges were scaled from the Mulliken charges in order to reproduce both the heats of adsorption in silicate and the solid CO structure realistically. The LJ potential for CO were assigned as  $\epsilon_{\text{Cco}} = 0.053 \text{ kcal mol}^{-1}$ ,  $\sigma_{\text{Cco}} = 4.012 \text{ \AA}$  and  $\epsilon_{\text{Oco}} = 0.085 \text{ kcal mol}^{-1}$ ,  $\sigma_{\text{Oco}} = 3.602 \text{ \AA}$ .<sup>41</sup>  $\text{CH}_4$  was represented by an atomic point charge model with the following partial charges carried by each atom (in electron units): C (−0.48e) and H (+0.12e). For  $\text{CH}_4$ , the LJ parameters  $\epsilon_{\text{H}} = 0.0152 \text{ kcal mol}^{-1}$ ,  $\sigma_{\text{H}} = 3.19 \text{ \AA}$ ,  $\epsilon_{\text{C}} = 0.0713 \text{ kcal mol}^{-1}$ , and  $\sigma_{\text{C}} = 3.9 \text{ \AA}$  were taken.<sup>42,43</sup>

The zeolite framework oxygen, silicon, and aluminum and the extra framework cations served as both the LJ interaction

**Table 1.** Pair Potential Parameters Used for Adsorbates ( $N_2$ , CO and  $CH_4$ ) and Adsorbent in the Simulation

interacting pairs	CO		Interacting pairs	$CH_4$		Interacting pairs	$N_2$	
	$\epsilon$ (kcal mol $^{-1}$ )	$\sigma$ (Å)		$\epsilon$ (kcal mol $^{-1}$ )	$\sigma$ (Å)		$\epsilon$ (kcal mol $^{-1}$ )	$\sigma$ (Å)
Oco–Oco	0.085	3.602	C–C	0.0713	3.900	N–N	0.0724	3.318
Cco–Cco	0.053	4.012	H–H	0.0152	3.190	N–Oz	0.1555	3.179
Oco–Cco	0.067	3.807	Oz–C	0.1149	3.589	N–Li	0.2282	2.208
Cco–Oz	0.133	3.526	Oz–H	0.0811	3.250	N–Na	0.0851	2.516
Oco–Oz	0.168	3.321	Na–H	0.0390	2.468	N–K	0.0804	2.803
Cco–Li	0.195	2.555	Na–C	0.0844	2.823	N–Rb	0.7630	2.908
Oco–Li	0.247	2.345	Li–H	0.3046	2.144	N–Cs	0.7420	3.021
Cco–Na	0.799	2.599	Li–C	0.4295	2.499			
Ooc–Na	0.101	2.400	K–H	0.4027	2.739			
Cco–K	0.029	3.150	K–C	0.5101	3.094			
Oco–K	0.047	2.945	Rb–H	0.3028	2.844			
Cco–Rb	0.053	3.255	Rb–C	0.4102	3.199			
Oco–Rb	0.227	3.050	Cs–H	0.2728	2.957			
Cco–Cs	0.003	3.268	Cs–C	0.3802	3.312			
Oco–Cs	0.020	3.1631						

site and the location of point charge. The LJ parameters used for the interactions of adsorbate–adsorbate and adsorbate–zeolite framework are given in Table 1. The calculation requires LJ parameters for the oxygen of the framework, extra framework cations and adsorbates because of considering that the polarizability of silicon and aluminum are much lower than those of oxygen atoms, therefore the non bond interactions are assigned only for framework oxygen and extra framework cations of the adsorbent in the modeling calculation. The parameter for framework oxygen was taken from literatures.<sup>27,42,43</sup> Maurin et al.<sup>27</sup> has suggested a relationship between ionic radius and polarizability<sup>44–45</sup> of cation to deduce the LJ parameter for each cation. The energy parameters were slightly adjusted to get the experimental heat of adsorption due to the understanding of the potential variation of cation in the zeolite framework. Table 1 summarizes the various potential parameters used in this work. The cations in the framework were assumed to be partially ionized and their charges were treated as adjustable parameters. The partial charges on silicon (+2.4e) and oxygen (−1.2e) of the zeolite framework system were fixed at the usually considered values.<sup>46</sup> The partial charges for aluminum atoms and alkali metal cations were taken as +1.7e and +0.7e respectively, which is also usually considered partial charges for aluminum and extra framework cations in the faujasite type zeolites.<sup>27</sup> The LJ parameters and partial charges were selected by adjusting to get the experimentally observed adsorption energy. The packing of adsorbate molecules around the cation in zeolite cavity could be determining the capacity of particular gas. So the adsorption entropy could define the adsorption capacity of gases in zeolites. However, the simulation studies were calculated without considering entropy factor. Furthermore, the simulations were calculated using perfect crystalline materials and the location of cation in zeolites as reported in the literature.

The absolute isotherms were then computed using Grand Canonical Monte Carlo (GCMC) algorithm via the “Sorption” module in the Materials Studio software (MS 4.3), which allows displacements, creations, and destructions of adsorbate species. All these simulations were performed with fixed pressures at 288.2 and 303.2 K using one unit cell of each model with a typical number of Monte Carlo steps ranging from 4 to 5 millions. The evolution of the total energy over the Monte Carlo steps were plotted in order to monitor the equilibration conditions. The zeolite structure was assumed to be rigid during the sorption process and the extra framework cations were maintained fixed in their initial optimized positions. Ewald summation method<sup>47</sup> was used for calculating the electrostatic interactions and the short-range interactions, with a cutoff distance

of 12.5 Å. The GCMC method allows for the insertion of molecules throughout the zeolite framework regardless of the physical diffusion pathways. Sorbate molecules such as  $CH_4$ ,  $N_2$ , and CO, due to their larger size, cannot be adsorbed into the sodalite cages, and therefore, dummy atoms of zero mass and charge were placed at the center of the sodalite cages to prevent the introduction of these molecules inside these cages.

#### 4. Results and Discussion

The X-ray powder diffractions of the alkali metal cation-exchanged zeolite samples reported in Figure 1, the retention of the zeolite structure after the cation exchange as the major  $2\theta$  diffractions typically observed for zeolite-X ( $2\theta = 6.1, 10.0, 15.5, 20.1, 23.4, 26.7, 29.3, 30.5, 31.0$ , and  $32.1$ ). The unit cell composition and the percentage crystallinity for the various cation-exchanged zeolite samples are given in Table 2.

The equilibrium adsorption capacities for the adsorption of CO,  $CH_4$  and  $N_2$  on zeolite-X containing different alkali metal ions are determined from the adsorption isotherm, and the number of molecule per unit cell of various alkali metal ions exchanged zeolite-X at 101.3 kPa and two different temperatures of 288.2 and 303.2 K are given in Table 3. The adsorption isotherms of CO,  $CH_4$  and  $N_2$  in alkali metal cation ( $Li^+$ ,  $Na^+$ ,  $K^+$ ,  $Rb^+$  and  $Cs^+$ ) containing zeolite-X at 303.2 K are shown in Figure 2. The adsorption capacity for CO and  $CH_4$  is higher in all alkali metal cation exchanged zeolites compared to the

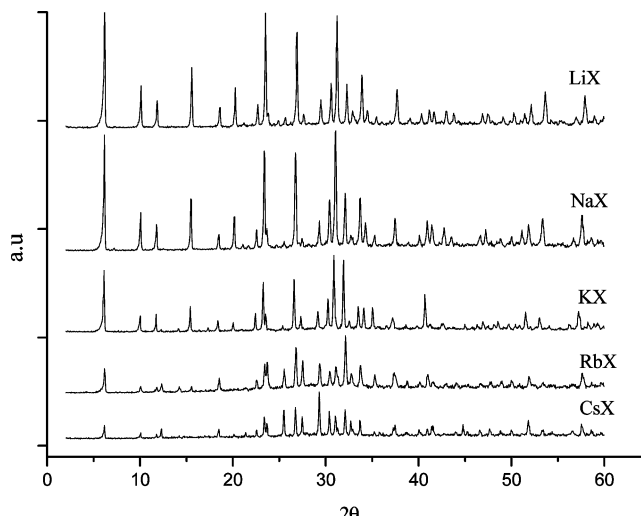


**Figure 1.** X-ray powder diffraction pattern of alkali metal cation exchanged zeolite-X.

**Table 2. Unit Cell Composition and Percentage Crystallinity of Alkali Metal Cation Exchanged Zeolites**

adsorbent	% exchange	unit cell composition (on anhydrous basis)	% crystallinity	BET surface area ( $\text{m}^2 \text{ g}^{-1}$ )	pore volume ( $\text{cm}^3 \text{ g}^{-1}$ )
NaX	100	$\text{Na}_{88}\text{Al}_{88}\text{Si}_{104}\text{O}_{384}$	100	721	0.36
LiX	95	$\text{Li}_{83.6}\text{Na}_{4.4}\text{Al}_{88}\text{Si}_{104}\text{O}_{384}$	90	759	0.33
KX	98	$\text{K}_{86.24}\text{Na}_{1.76}\text{Al}_{88}\text{Si}_{104}\text{O}_{384}$	95	537	0.26
RbX	86	$\text{Rb}_{75.68}\text{Na}_{12.32}\text{Al}_{88}\text{Si}_{104}\text{O}_{384}$	85	550	0.21
CsX	84	$\text{Cs}_{73.92}\text{Na}_{14.08}\text{Al}_{88}\text{Si}_{104}\text{O}_{384}$	86	423	0.19

**Table 3. Equilibrium Adsorption Capacity for CO, CH<sub>4</sub> and N<sub>2</sub> in Alkali Metal Cation Exchanged Zeolite-X**

adsorbent	equilibrium adsorption capacity, molecule/unit cell at 101.3 kPa					
	288.2 K			303.2 K		
	CO	CH <sub>4</sub>	N <sub>2</sub>	CO	CH <sub>4</sub>	N <sub>2</sub>
LiX	22.4	10.1	9.2	16.9	9.9	7.0
NaX	21.2	13.7	7.7	15.3	10.1	5.5
KX	12.9	17.8	5.4	8.9	12.6	4.0
RbX	11.2	16.5	5.6	7.8	12.4	4.1
CsX	10.9	21.1	5.5	7.9	14.9	3.8

adsorption capacity of N<sub>2</sub>. It can be seen from the Figure 2 that lithium-exchanged zeolite-X shows highest adsorption capacity for CO at 101.3 kPa and 303.2 K than the other alkali metal ion exchanged zeolite-X. Furthermore, it can be observed that the adsorption capacity decreases in the sequences LiX > NaX > KX > CsX for both CO and N<sub>2</sub> following in alkali metal series on decreasing of the ionic radius of the extra framework cations. In the case of CO (Figure 2a), the adsorption capacity decreases as the cation radius increases. The adsorption of polar CO is higher than the quadrupolar N<sub>2</sub> molecule.<sup>48</sup> Thus electrostatic interaction between smaller Li cation and CO molecules is very high at initial stages of adsorption. The CH<sub>4</sub> adsorption capacity increases on increasing cationic radius, which has reverse order of ionic radius of extra framework cations.

The nonpolar Ar adsorption shows the affinity in the decreasing order of cation size,<sup>49</sup> but the nonpolar CH<sub>4</sub> molecules adsorption in alkali metal exchanged zeolites-X increase with increase in extra framework cation radius. The extra framework cations in the zeolite cavities are preferred adsorption sites for interacting with polar or easily polarizable molecules. It has also been seen that the nature of cation will affect the adsorption of nonpolar molecules due to the induced electrostatic interactions of the ionic surface.<sup>50</sup> Talu et al.<sup>28</sup> has reported the adsorption affinity of CH<sub>4</sub> in the alkaline earth metal ion exchanged zeolites-X and -Y with increasing order of cation size at wide range of pressures. These observations were explained by possible shielding of small cation by the first few molecules of a cavity (first shell of adsorbates), which would limit the interaction with adsorbate molecules. The larger cation would not experience this shielding and hence would be able to affect larger number of molecules in the outer shell, even though the imposed potential is smaller than that imposed by a Li cation. Moreover, CO and N<sub>2</sub> molecules are linear in shape but the CH<sub>4</sub> molecule is spherical one, the end-on interaction of linear molecule with cation favors additional space to accommodate more adsorbate molecules around a particular cation located in the 6-membered ring of the zeolites. The spherical CH<sub>4</sub> molecule could shield the cations for interacting with higher number of molecules. Therefore, in the case of CH<sub>4</sub> adsorption, the exposure of particular cation located in the cavity could be hindered by the initially adsorbed molecules.

The pure component adsorption selectivity for CO and CH<sub>4</sub> over N<sub>2</sub> at different equilibrium pressures was calculated, and the values at 303.2 K are given in Table 4. The values of CO/N<sub>2</sub>, CH<sub>4</sub>/N<sub>2</sub>, and CH<sub>4</sub>/CO slightly decrease at higher pressures for each cation exchanged zeolites. The CO/N<sub>2</sub> selectivity

remains almost ~2.0 in all alkali metal exchanged zeolite-X at 1 atm pressure and 303.2 K. This could be due to the electrostatic interactions induced in the zeolites by both polar and quadrupolar gases of being approximately same magnitude. The CH<sub>4</sub>/N<sub>2</sub> selectivity decreases in the order of increasing cation radius. Table 4 shows the adsorption selectivity of CH<sub>4</sub>/N<sub>2</sub> and CO/N<sub>2</sub> in alkali metal ion exchanged zeolite-X at 303.2 K. The pure component adsorption selectivity of CO over CH<sub>4</sub> is also reported in Table 4, which indicates the selectivity of CO and CH<sub>4</sub> gets reversed on increasing cation radius. Both LiX and NaX show selectivity of CO over CH<sub>4</sub>, but rest of the alkali metal exchanged zeolites shows CH<sub>4</sub> over CO.

Simulation of the adsorption CO, N<sub>2</sub> and CH<sub>4</sub> in alkali metal ion exchanged zeolite-X were carried out at two different temperatures 288.2 and 303.2 K. Figure 3 shows both experimental and simulated adsorption isotherms of CO, N<sub>2</sub> and CH<sub>4</sub> in zeolite-X having alkali metal extra framework cations at 303.2 K. It is clear from the Figure 3 that the simulation of CO, N<sub>2</sub> and CH<sub>4</sub> isotherm of alkali metal ion exchanged zeolite-X predicts the experimental results reasonably well. It can be seen that the simulated adsorption isotherm matches well with experimental data for NaX, but for other cation exchanged zeolite-X, experimental values are lower than theoretically predicted values. The different values for the simulated and experimental adsorption isotherms for the exchanged zeolites could be due to the fact that there is decrease in the crystallinity of alkali metal ion exchanged zeolite as shown in Table 2 or/and due to underestimated parameter selection for simulation. The simulated adsorption isotherms of CO and CH<sub>4</sub> show higher values compared to the experimental data. The discrepancy in simulation isotherm with experimental one could be due to the cationic location changing from sorbate accessible site to less accessible site during the activation time, whereas the simulation were carried out by using the cationic site reported in literature. Furthermore, the adsorbent used for the experiments could have minor quantities of other phases formed during the synthesis of zeolite powders, and however we used single unit cell of the zeolite for the simulation. Moreover, this could be due to the strong interaction of hydrated cations to zeolite structure that can result to some structural defects or formation of amorphous phase, probably due to dealumination during the cation exchange or vacuum dehydration process. This is also evidenced by the decrease in the crystallinity of samples with alkali metal cation exchanged zeolite as shown in Table 2.

The isosteric heats of adsorption for CO, N<sub>2</sub> and CH<sub>4</sub> in alkali metal zeolite-X, calculated from both experimental and simulated at 1 molecule/u.c are given in Table 5. From the table it can be seen that the heat of adsorption of the polar and quadrupolar gases decreases as charge density of the extra framework cation decreases, i.e., increasing cation size. As increase in cation size of alkali metal cation, the heats of adsorption decreases from 28 to 19 kJ mol<sup>-1</sup> and from 24.7 to 15.6 kJ mol<sup>-1</sup> for CO and N<sub>2</sub>, respectively. In the case of CH<sub>4</sub>, heat of adsorption does not show much decrease (23.6 to 20.7 kJ mol<sup>-1</sup>) with increase in cation size, as moving from Li to Cs extra-framework cations. The heats of adsorption of CO, N<sub>2</sub> and CH<sub>4</sub> at different coverages in various alkali metal cation

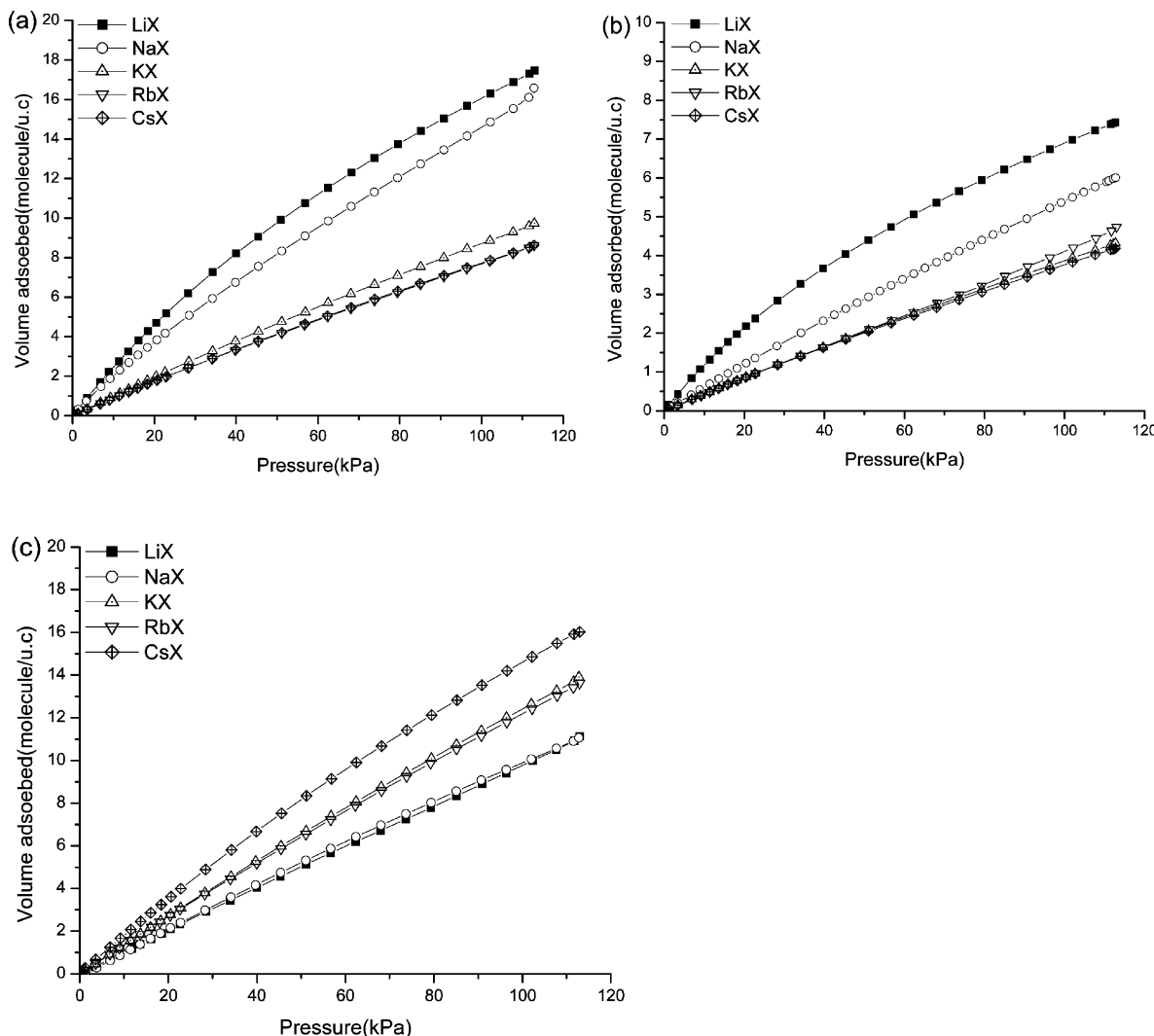


**Figure 2.** Experimental adsorption isotherm of alkali metal ion exchanged zeolite-X for (a) CO, (b) N<sub>2</sub>, and (c) CH<sub>4</sub> at 303.2 K.

**Table 4. CO/N<sub>2</sub>, CH<sub>4</sub>/N<sub>2</sub> and CO/CH<sub>4</sub> Pure Component Adsorption Selectivity on Alkali Metal Cation Exchanged Zeolite-X at 303.2 K**

adsorbent	CO/N <sub>2</sub>		pure component adsorption selectivity			
	3.33 kPa	101.99 kPa	3.33 kPa	101.99 kPa	3.33 kPa	101.99 kPa
LiX	1.75	2.41	1.35	1.41	2.27	1.71
NaX	2.33	2.78	1.41	1.82	2.42	1.51
KX	2.31	2.23	3.23	3.15	0.71	0.69
RbX	2.41	1.95	3.71	3.05	0.65	0.63
CsX	2.18	2.08	4.61	3.92	0.47	0.53

exchanged zeolites are shown in Figure 4. The heats of adsorption reasonably well predicted in simulation, however the amounts of gases adsorbed in zeolites is not predicted well. This could be due to the fact that adsorption isotherms were calculated without considering the entropy factor in simulation studies.

Zeolite-X is a synthetic aluminum rich analogue of the naturally occurring mineral faujasite. The 14-hedron with 24 vertices known as the sodalite cavity or  $\beta$ -cage may be viewed as its principal building block. These  $\beta$ -cages are connected tetrahedrally at six-rings by bridging oxygen to give double six-rings (D6Rs, hexagonal prisms) and concomitantly, an interconnected set of even larger cavities (supercage) accessible in three dimensions through 12-ring (24-membered) windows.<sup>21</sup> The extra framework cations are usually found at the following sites as shown in Figure 5. In the framework diagram of zeolite-X, near the center of the each line segment is an oxygen atom.

The numbers 1–4 indicate the different oxygen atoms. Extra framework cation positions are labeled with Roman numerals, site I at the center of the D6R, I' in the sodalite cavity on the opposite side of one of the D6Rs six-rings from site I, II' inside the sodalite cavity near a S6R, II at the center of the S6R or displaced from this point into a supercage, III in the supercage on a 2-fold axis opposite a four-ring between two 12-rings, and III' somewhat or substantially off III (off the 2-fold axis) on the inner surface of the supercage

In the case of dehydrated NaX, the site occupancies on a unit cell basis are as follows: site I' = 30, site II = 28, and 30 cations are distributed in sites III and III'.<sup>22</sup> Out of these four sites, site II and III, which are in the supercage, are accessible to the CO, N<sub>2</sub>, and CH<sub>4</sub> molecules. In lithium exchanged zeolite-X, out of 88 Li<sup>+</sup> ions, 30 ions occupy site I, 28 ions are in site II, and the remaining 30 ions occupy sites III and III'.<sup>29</sup> The site occupancy of fully exchanged KX,<sup>30</sup> RbX,<sup>31</sup> and CsX<sup>32</sup> are

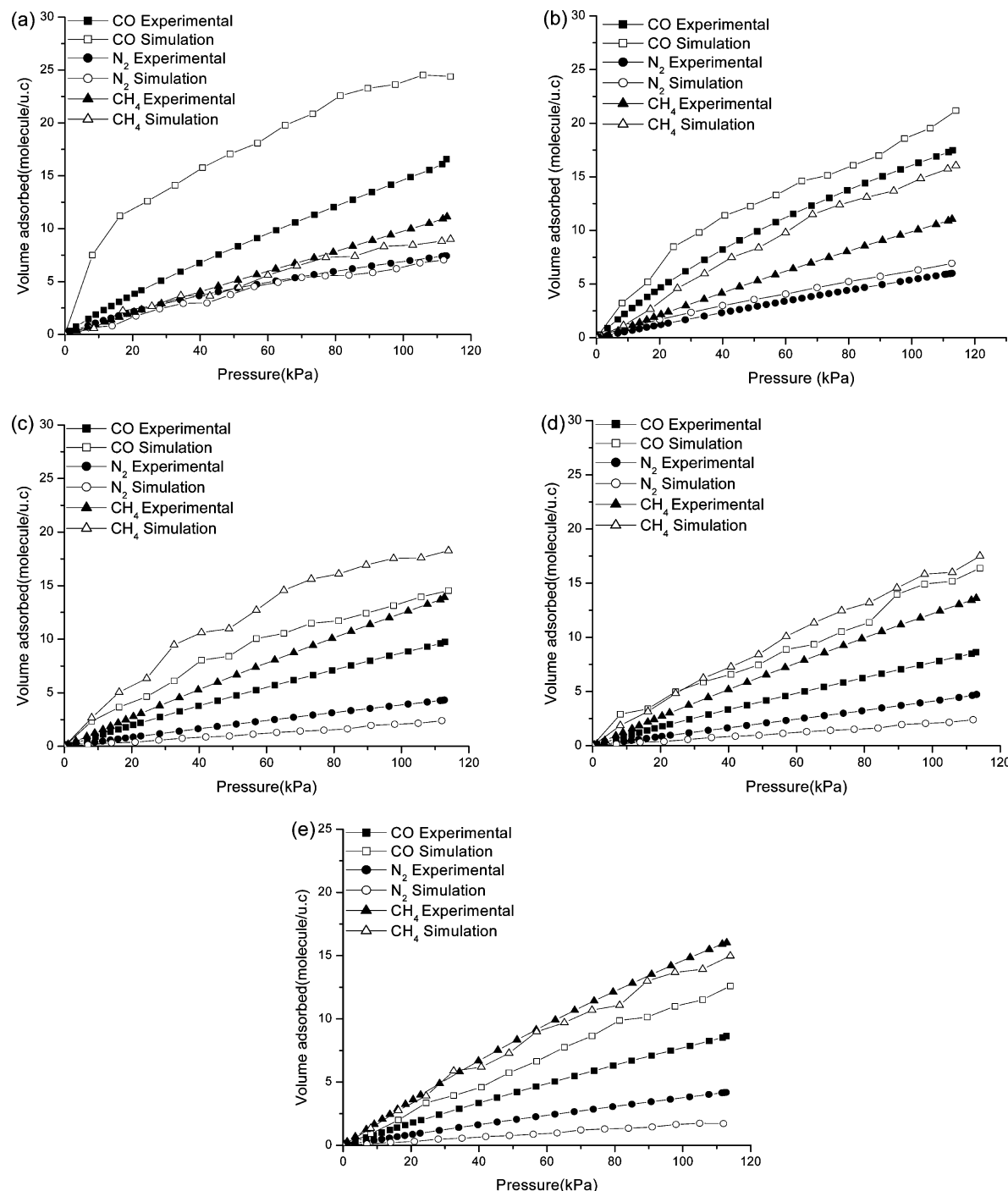


**Figure 3.** Experimental and simulated adsorption isotherms of CO, N<sub>2</sub>, and CH<sub>4</sub> in (a) LiX, (b) NaX, (c) KX, (d) RbX, and (e) CsX at 303.2 K.

**Table 5. Isosteric Heats of Adsorption on Alkali Metal ion Exchanged Zeolites at 1 molecule/u.c. Coverage**

adsorbent	heat of adsorption (kJ mol <sup>-1</sup> )					
	experimental			simulated		
	CO	N <sub>2</sub>	CH <sub>4</sub>	CO	N <sub>2</sub>	CH <sub>4</sub>
LiX	31.2	24.7	23.6	33.3	25.3	23.4
NaX	26.1	21.5	21.5	28.9	22.6	21.8
KX	21.3	17.3	20.8	21.9	14.5	20.2
RbX	20.1	16.0	20.8	19.0	18.1	20.4
CsX	19.2	15.6	20.7	19.0	13.9	20.4

as reported in the literature.<sup>29–32</sup> In the case of the unit cell structure, some of the cavities were inaccessible to these gases for adsorption because of the blockage of an extra framework cation located at site-I. In the case of crystal structure of

dehydrated alkali metal ion exchanged zeolite-X, the framework bond angles are similar to those in NaX. Thus the adsorption behavior of both cation exchanged and sodium forms of zeolite-X is expected to have the same adsorption properties. The variations in the adsorption behavior toward CO, N<sub>2</sub>, and CH<sub>4</sub> are due to the differences in the interactions of extra-framework cations with these adsorbate molecules.

The interactions between zeolite and adsorbed molecule such as CO, N<sub>2</sub>, and CH<sub>4</sub> involve electrostatic, induction, dispersion, and short-range repulsive forces. The electrostatic interaction arises between the adsorbed molecules possessing dipole or quadrupole moments and permanent electric field of the zeolite. The permanent electric field depends on the nature of the cations and their location in the zeolite cavity. Therefore, the heat of

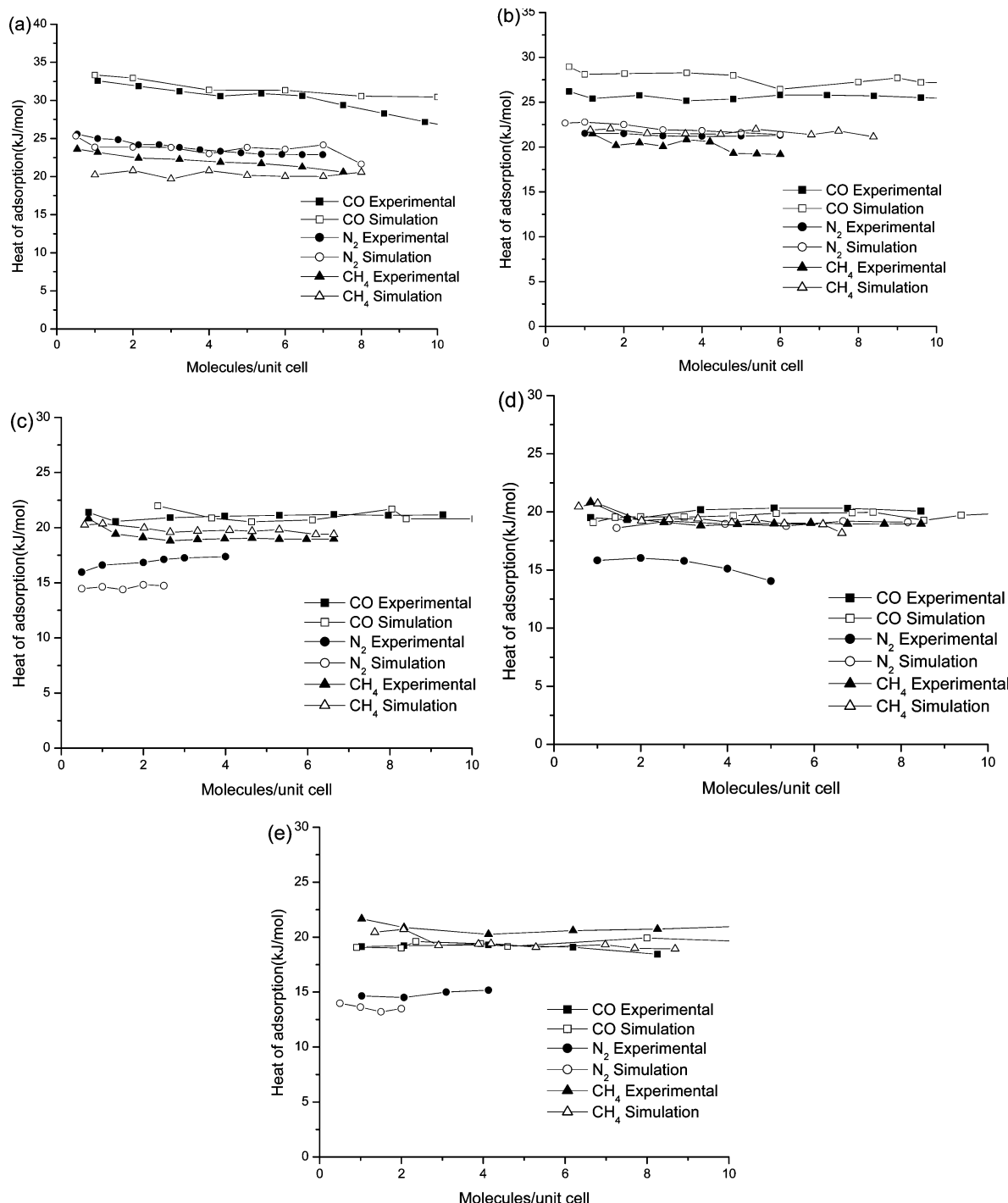


**Figure 4.** Experimental and simulated heats of adsorption of CO, CH<sub>4</sub>, and N<sub>2</sub> at different coverage in (a) LiX, (b) NaX, (c) KX, (d) RbX, and (e) CsX.

adsorption for both CO and N<sub>2</sub> decreases on increasing the cation size of the extra framework cation. The charge density decreases on increasing the cation radius because strength of electrostatic interaction of adsorbate with cation gets reduced on increasing cation size in the zeolite cavity. The cations present in the supercages can interact easily with the guest molecules than the cations present in other cage. As the size of extra framework cation increases, the interaction between the cations and guest molecules decreases which led to increase the distance between sorbate molecule and extra framework cations.

In a zeolite framework, SiO<sub>2</sub> and AlO<sub>2</sub> tetrahedra are connected by sharing oxygen atoms. Al and Si atoms are buried in the tetrahedra of oxygen atoms and are not directly exposed

to sorbate molecules. Thus, the main interactions of the adsorbate molecules in a zeolite structure are through lattice oxygen atoms and extra framework cations. The cations are the preferred adsorption sites that are especially important for interacting with polar, quadrupolar and easily polarizable molecules. The CO molecule possesses both dipole moment and quadrupole moment (Table 6). Therefore, the CO molecules can have stronger interaction with high charge density Lithium cation containing zeolites. The dominant interaction between the CO molecules and cations are electrostatic, which is mainly driven by dipole as well as quadrupole moment of CO molecule. Because of this the heats of adsorption and adsorption capacity decrease in the order of decreasing cation size in alkali metal ion exchanged zeolite-X samples. The simulation performed on

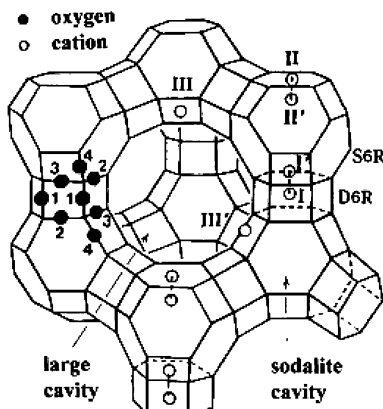


**Figure 5.** Framework structure of zeolite-X.

**Table 6. Molecular Properties of Adsorbates**

	CO	N <sub>2</sub>	CH <sub>4</sub>
dipole moment ( $\times 10^{-31}$ C m)	3.7	0	0
quadrupole moment ( $\times 10^{-40}$ C <sup>2</sup> m <sup>2</sup> )	-6.7	-5.0	0
polarizability ( $\times 10^{-40}$ C <sup>2</sup> m <sup>2</sup> J <sup>-1</sup> )	2.2	2.0	2.6

a pure unit cell structures for alkali metal exchanged zeolite-X without any structural defects, which reproduces the adsorption capacity and heats of adsorption in the order of LiX > KX > RbX > CsX as the same trend as shown in experimental results. Figure 6 shows the unit cell structures of alkali metal ion exchanged zeolite-X adsorbed with CO at 101.3 kPa and 303.2 K. In the case of all alkali metal containing zeolites, CO molecules are sitting close to cations located in site II, at the center of the six member ring and also in site III', inside the supercage as can be seen from the figure. Furthermore, our simulation emphasized on increasing the cationic size of the alkali metal cation in zeolite-X the interaction between CO and cations are weakened, therefore the population of CO molecule in supercages is reduced in the order of LiX > NaX > KX > RbX > CsX. The simulated structure also reveals the distance between the CO and cation increases on increasing the cation size in the zeolites.

In the case of N<sub>2</sub> molecule also, the dominant interaction between the N<sub>2</sub> molecules and cations could be due to the electrostatic contribution, which is mainly driven by the

quadrupole moment of N<sub>2</sub> molecule. Figure 7 shows the unit cell structures of alkali metal ion exchanged zeolite-X adsorbed with N<sub>2</sub> at 101.3 kPa and 303.2 K. Simulation studies indicate that in the case of N<sub>2</sub> molecule two adsorption sites i.e close to cations located in site II, at the center of the six member ring and also in site III', inside the supercage as can be seen from the Figure 7 are observed. The N<sub>2</sub> molecules are occupied mainly in supercages, interacting strongly with the cations located in supercages. Simulation studies also shows the heat of adsorption and adsorption capacity decrease on increasing cation size, and N<sub>2</sub> molecules decrease in supercages in the order LiX > NaX > KX > RbX > CsX. The charge density of cation inside the supercage is main contributor towards the electrostatic interaction of N<sub>2</sub> molecule and alkali metal ion containing zeolite-X. Due to the higher charge density of smaller cations the distance between the center of N<sub>2</sub> molecule and cation is smaller in the case of lithium exchanged zeolites. The distance of the N<sub>2</sub> molecule from cation increases on increasing the cation size. Among the three gases, N<sub>2</sub> has the lowest polarizability; as a result, the polarization contribution toward the adsorption is less in the case of N<sub>2</sub> adsorption in alkali metal ion exchanged zeolites.

The polarizability of CH<sub>4</sub> molecule is higher than that of CO and N<sub>2</sub> so that the heats of adsorption decrease on decreasing the polarization power of alkali metal cation in zeolite-X (i.e. LiX > NaX > KX > RbX > CsX). The heat of adsorption for CH<sub>4</sub> is also driven by the electrostatic interactions. At low pressure region, the prominent interaction of sorbate with zeolite framework is dispersive compared to the electrostatic contribution because of that the heat of adsorption of CO and CH<sub>4</sub> is higher than N<sub>2</sub> on each alkali metal exchanged zeolite-X. However, the higher heat of adsorption of CO on LiX and NaX than CH<sub>4</sub> is due to the higher electrostatic interaction of CO molecules toward the very high charge density of Li and Na. The heat of adsorption indicates the strength of CH<sub>4</sub>/zeolite-X interactions; such decreases in heat of adsorption with decreasing charge density indicate the smaller cations are good enough to produce a strong electrostatic field to polarize the symmetric CH<sub>4</sub> molecule. The adsorption capacity is in reverse order of the polarizing power of alkali metal ion in cation exchanged zeolite-X, i.e., in the order CsX > RbX > KX > NaX > LiX. This is due to the shielding effect of the initially adsorbed CH<sub>4</sub>.

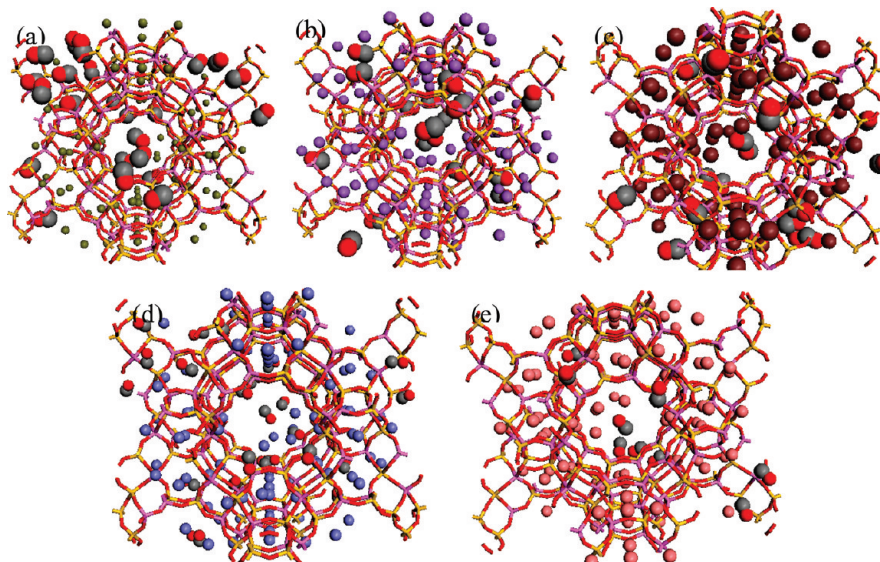


**Figure 6.** Molecular graphic snapshot of CO adsorbed unit cell of (a) LiX, (b) NaX, (c) KX, (d) RbX, and (e) CsX at 101.3 kPa and 303.2 K.

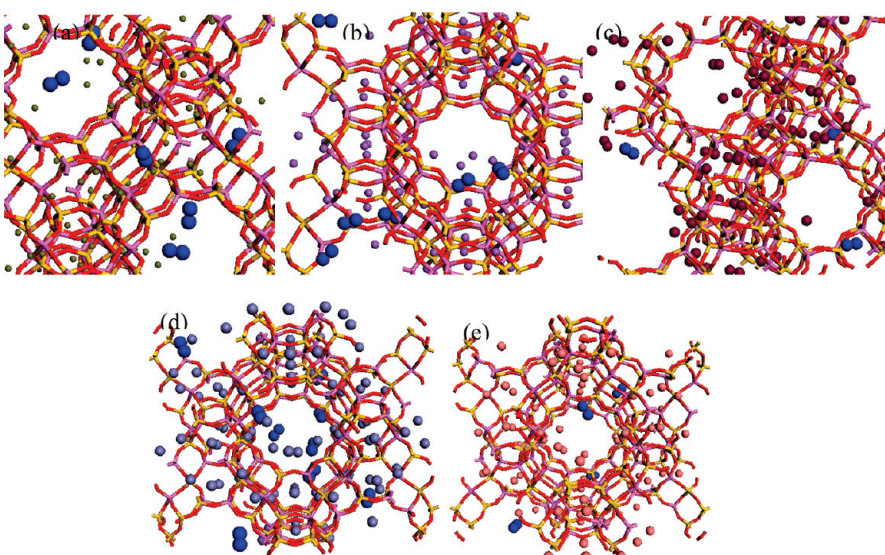


**Figure 7.** Molecular graphic snapshot of  $\text{N}_2$  adsorbed unit cell of (a) LiX, (b) NaX, (c) KX, (d) RbX, and (e) CsX at 101.3 kPa and 303.2 K.

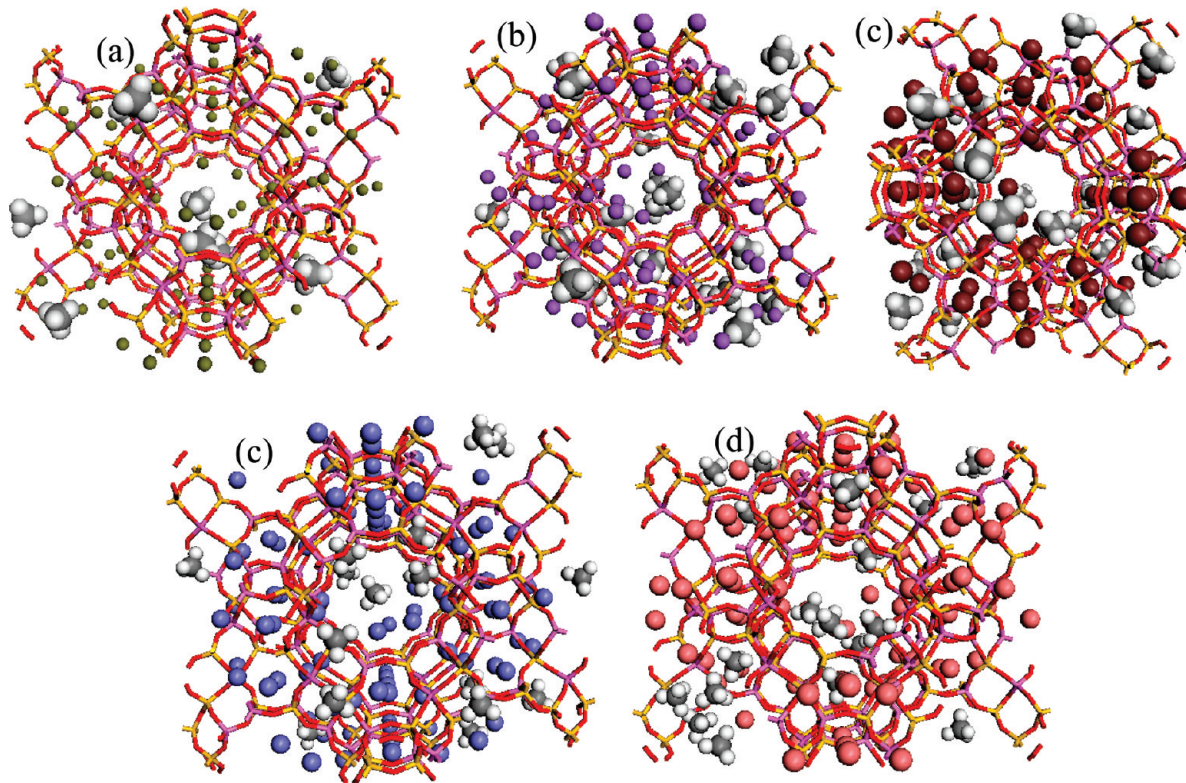


**Figure 8.** Molecular graphic snapshot of  $\text{CH}_4$  adsorbed unit cell of (a) LiX, (b) NaX, (c) KX, (d) RbX, and (e) CsX at 101.3 kPa and 303.2 K.

molecules on the metal ion as postulated by Talu et al.<sup>28</sup> The simulation studies of  $\text{CH}_4$  adsorption on zeolites shows the single  $\text{CH}_4$  molecule can get closer to the cation in the order of  $\text{Li} > \text{Na} > \text{K} > \text{Rb} > \text{Cs}$ . Thus the  $\text{CH}_4$  heats of adsorption of smaller cations are higher and the distance between center of  $\text{CH}_4$  molecule and cation increases on increasing cation size in zeolite-X. Figure 8 shows the  $\text{CH}_4$  adsorbed unit cell structure for all alkali metal exchanged zeolite-X at 101.3 kPa and 303.2 K. Simulation studies reveal on increasing loading an initial shell of adsorbate are covered on the cations, which are known as ‘first shell’. The molecules in the ‘first shell’ determine the potential of adsorption, which means the smaller cations impose a strong potential but only for limited number of molecules. The larger cations can impose lower potential but for a large

number of molecules as shown in Figure 8. Therefore, the heat of adsorption is slightly higher for the smaller cation exchanged zeolite-X but the adsorption capacity is higher for the bigger cation containing zeolite-X. The strong interaction of  $\text{CH}_4$  molecules with smaller cations releases more heat as compared to bigger cations during  $\text{CH}_4$  adsorption in alkali metal ion exchanged zeolite-X. The simulated structure shows the distance between smaller cations and  $\text{CH}_4$  molecules are shorter than the bigger cations.

## Conclusions

Equilibrium adsorption measurements of the sorption of  $\text{CO}_2$ ,  $\text{N}_2$ , and  $\text{CH}_4$  are performed in zeolite-X with various alkali metal

ions. The alkali metal ion containing zeolite-X shows higher adsorption capacity for CO and CH<sub>4</sub> than N<sub>2</sub>. The adsorption capacity of CO in alkali metal exchanged zeolites decreases on increasing ionic radius, while for CH<sub>4</sub> the adsorption capacity increases on increasing extra framework cationic radius. Isosteric heat of sorption data show stronger interactions of CO and N<sub>2</sub> molecules with alkali metal ion exchanged zeolites and which is decreases on increasing size of the cation. The isosteric heat of CH<sub>4</sub> is approximately equal for all alkali metal ion containing zeolites. Simulation of the CO and N<sub>2</sub> sorption in alkali metal zeolite-X clearly shows that, the adsorbed CO and N<sub>2</sub> molecules sit closely to the extra-framework cations accessible through the super cage. Simulation of adsorption isotherms and heats of adsorption of CO, N<sub>2</sub>, and CH<sub>4</sub> in alkali metal ion exchanged zeolite-X match reasonably well with the experimental results.

## Acknowledgment

We greatly admire the financial assistance and support from Council of Scientific and Industrial Research (CSIR), New Delhi. R.S.P and G.S thank the CSIR, New Delhi, India, for financial assistance in the form of senior research fellowship. We also thank Dr. Casten Menke, and Dr. Alexandra Simperler Accelrys, E.U., for their fruitful discussion in molecular simulation.

**Supporting Information Available:** Text discussing the measurement of N<sub>2</sub>, CH<sub>4</sub>, and CO adsorption isotherms and figures showing them. This material is available free of charge via the Internet at <http://pubs.acs.org>.

## Literature Cited

- (1) Cavenati, S.; Grande, C. A.; Rodrigues, A. E. *J. Chem. Eng. Data* **2004**, *49*, 1095–1101.
- (2) BP Statistical Review of World Energy, 2005 ([www.bp.com](http://www.bp.com), accessed in August 2005).
- (3) Nicholas, D. M.; Goff, S. P.; Roden, T. M.; Bushinsky, J. P. U.S Patent 4,836, 833, 1989.
- (4) Nakao, G.; Ishisaka, H.; Takamoto, S.; Nishimura, Y. U.S Patent 4,950,462, 1990.
- (5) Cavenati, S.; Grande, C. A.; Rodrigues, A. E. *Sep. Sci. Technol.* **2005**, *40*, 2721–2743.
- (6) US EPA Doc 430-R-97-012, Technical and Economic Assessment of Potential to Upgrade Gob Gas to Pipeline Quality. December 1997, 199–204. ([www.epa.gov](http://www.epa.gov), accessed in August 2005)
- (7) Shires, P. J.; Cassata, J. R.; Mandelik, B. G.; van Dijk, C. P. U.S Patent 4,479,925, 1984.
- (8) <http://www.epa.gov/methane/index.html>, <http://www.epa.gov/ebtpages/airairpollutantsmethane.html>
- (9) Jayaraman, A.; Hernández-Maldonado, A. J.; Yang, R. T.; Chinn, D.; Munson, C. L.; Mohr, D. H. *Chem. Eng. Sci.* **2004**, *59*, 2407–2417.
- (10) Engelhard Corporation, *Adsorption Processes for Natural Gas Treatment, A Technology Update*; [www.engelhard.com](http://www.engelhard.com), 2005.
- (11) Alleyne, D. H. N. The state Petroleum Enterprise and transfer of technology. In *United Nations Centre for Natural Resources, Energy and Transport (UNCNRET), state petroleum enterprises in developing countries*; Pergamon Press: New York, 1980.
- (12) Ruthven, D. M. *Principles of Adsorption and Adsorption Processes*; Wiley: New York, 1984.
- (13) Ruthven, D. M., Farooq, S., Knaebel, K. S. *Pressure Swing Adsorption*; VCH Publishers: New York. 1994.
- (14) Yang, R. T. *Gas Separation by Adsorption Processes*; Butterworths: Boston, MA, 1987.
- (15) Breck, D. W. *Zeolite Molecular Sieves: Structure, Chemistry and Use*; Wiley: New York, 1974.
- (16) Yang, R. T. *Adsorbents: Fundamentals and Applications*; Wiley-Interscience: New York, 2003.
- (17) Jain, R. U.S Patent 5,551,257, 1996.
- (18) Cavenati, S.; Grande, C. A.; Rodrigues, A. E. *Chem. Eng. Sci.* **2006**, *61*, 3893–3906.
- (19) Prasanth, K. P.; Pillai, R. S.; Bajaj, H. C.; Jasra, R. V.; Chung, H. D.; Kim, T. H.; Song, S. D. *Int. J. Hydrogen Energy* **2008**, *33*, 735–745.
- (20) Sebastian, J.; Peter, S. A.; Jasra, R. V. *Langmuir* **2005**, *21*, 11220–11225.
- (21) Olson, D. H. *Zeolites* **1995**, *15*, 439–443.
- (22) Zhu, L.; Seff, K. *J. Phys. Chem. B* **1999**, *103*, 9512–9518.
- (23) Sebastian, J.; Pillai, R. S.; Peter, S. A.; Jasra, R. V. *Ind. Eng. Chem. Res.* **2007**, *46*, 6292–6302.
- (24) Peter, S. A.; Sebastian, J.; Jasra, R. V. *Ind. Eng. Chem. Res.* **2005**, *44*, 6856–6864.
- (25) Pillai, R. S.; Peter, S. A.; Jasra, R. V. *Langmuir* **2007**, *23*, 8899–8908.
- (26) Savitz, S.; Myers, A. L.; Gorte, R. J. *Microporous Mesoporous Mater.* **2000**, *37*, 33–40.
- (27) Maurin, G.; Llewellyn, P.; Poyet, T.; Kuchta, B. *J. Phys. Chem. B* **2005**, *109*, 125–129.
- (28) Talu, O.; Zhang, S.-Y.; Hayhurst, D. T. *J. Phys. Chem.* **1993**, *97*, 12894–12898.
- (29) Plévert, J.; Di Renzo, F.; Fajula, F.; Chiari, G. *J. Phys. Chem. B* **1997**, *101*, 10340–10343.
- (30) Zhu, L.; Seff, K. *J. Phys. Chem. B* **2000**, *104*, 8946–8951.
- (31) Lee, S. K.; Kim, D. S.; Kim, Y.; Seff, K. *Bull. Korean Chem. Soc.* **1998**, *19*, 98–103.
- (32) Ryu, K. S.; Bae, M. N.; Kim, Y.; Seff, K. *Microporous Mesoporous Mater.* **2004**, *71*, 65–75.
- (33) Razmus, D. M.; Hall, C. K. *AIChE J.* **1991**, *37*, 769–779.
- (34) Watanabe, K.; Austin, N.; Stapleton, M. R. *Mol. Simul.* **1995**, *15*, 197–221.
- (35) Hutson, N. D.; Zajic, S. C.; Yang, R. T. *Ind. Eng. Chem. Res.* **2000**, *39*, 1775–1780.
- (36) Richards, A. J.; Watanabe, K.; Austin, N.; Stapleton, M. R. *J. Porous Mat.* **1995**, *2*, 43–49.
- (37) Cerius<sup>2</sup> User Guide: Forcefield-Based Simulations; Molecular Simulations Inc.: San Diego, CA, April 1997.
- (38) Allen, M. P.; Tildesley, D. J. *Computer Simulation of Liquids*; Clarendon: Oxford, U.K., 1987.
- (39) Murthy, C. S.; Singer, K.; Klein, M. L.; McDonald, I. R. *Mol. Phys.* **1980**, *41*, 1387–1399.
- (40) Dmol3 v 4.2, Accelrys Inc.: San Diego, CA, 2008.
- (41) Yang, J.; Ren, Y.; Tian, A. *J. Phys. Chem. B* **2000**, *104*, 4951–4957.
- (42) Maurin, G.; Bourrelly, S.; Llewellyn, P. L.; Bell, R. G. *Microporous Mesoporous Mater.* **2006**, *89*, 96–102.
- (43) Maurin, G.; Bell, R.; Kuchta, B.; Poyet, T.; Llewellyn, P. *Adsorption* **2005**, *11*, 331–336.
- (44) Huheey, J. E.; Keiter, E. A.; Keiter, R. L. *Inorganic Chemistry: principles of structure and reactivity*, 4th ed.; Harper Collins College Publishers: New York, 1993.
- (45) Fratello, V. J.; Brandle, C. D. *J. Mater. Res.* **1994**, *9–10*, 2554–2562.
- (46) Kramer, G. J.; Farragher, N. P.; van Beest, B. W. H.; van Santen, R. A. *Phys. Rev. B* **1991**, *43*, 5068–5080.
- (47) Sorption, Materials Studio v 4.3; Accelrys Inc.: San Diego, CA, 2008.
- (48) Steele, W. *Chem. Rev.* **1993**, *93*, 2355–2378.
- (49) Maurin, G.; Llewellyn, P. L.; Poyet, T. H.; Kuchta, B. *Microporous Mesoporous Mater.* **2005**, *79*, 53–59.
- (50) Walton, K. S.; Abney, M. B.; Douglas LeVan, M. *Microporous Mesoporous Mater.* **2006**, *91*, 78–84.

Received for review October 31, 2009

Revised manuscript received March 27, 2010

Accepted April 13, 2010

IE901713M